



## Constraining masses and separations of unseen companions to five accelerating nearby stars

D. Mesa, M. Bonavita, S. Benatti, R. Gratton, S. Marino, P. Kervella, V. d'Orazi, S. Desidera, T. Henning, M. Janson, et al.

### ► To cite this version:

D. Mesa, M. Bonavita, S. Benatti, R. Gratton, S. Marino, et al.. Constraining masses and separations of unseen companions to five accelerating nearby stars. *Astronomy and Astrophysics - A&A*, 2022, 665, 10.1051/0004-6361/202244033 . insu-03780746

**HAL Id: insu-03780746**

**<https://insu.hal.science/insu-03780746>**

Submitted on 19 Sep 2022

**HAL** is a multi-disciplinary open access archive for the deposit and dissemination of scientific research documents, whether they are published or not. The documents may come from teaching and research institutions in France or abroad, or from public or private research centers.

L'archive ouverte pluridisciplinaire **HAL**, est destinée au dépôt et à la diffusion de documents scientifiques de niveau recherche, publiés ou non, émanant des établissements d'enseignement et de recherche français ou étrangers, des laboratoires publics ou privés.



Distributed under a Creative Commons Attribution 4.0 International License

# Constraining masses and separations of unseen companions to five accelerating nearby stars<sup>★</sup>

D. Mesa<sup>1</sup>, M. Bonavita<sup>1,2</sup>, S. Benatti<sup>3</sup>, R. Gratton<sup>1</sup>, S. Marino<sup>4,5</sup>, P. Kervella<sup>6</sup>, V. D' Orazi<sup>1</sup>, S. Desidera<sup>1</sup>, T. Henning<sup>7</sup>, M. Janson<sup>8</sup>, M. Langlois<sup>9,10</sup>, E. Rickman<sup>11,12</sup>, A. Vigan<sup>9</sup>, A. Zurlo<sup>13,14,9</sup>, J.-L. Baudino<sup>6</sup>, B. Biller<sup>7,15,16</sup>, A. Boccaletti<sup>6</sup>, M. Bonnefoy<sup>17</sup>, W. Brandner<sup>7</sup>, E. Buenzli<sup>7</sup>, F. Cantalloube<sup>9</sup>, D. Fantinel<sup>1</sup>, C. Fontanive<sup>18,1</sup>, R. Galicher<sup>6</sup>, C. Ginski<sup>19</sup>, J. Girard<sup>20,17</sup>, J. Hagelberg<sup>21</sup>, T. Kopytova<sup>7</sup>, A.-M. Lagrange<sup>6,17</sup>, C. Lazzoni<sup>1</sup>, H. Le Coroller<sup>9</sup>, R. Ligi<sup>22</sup>, M. Llored<sup>9</sup>, A.-L. Maire<sup>23,7</sup>, D. Mouillet<sup>17</sup>, C. Perrot<sup>6</sup>, S. Rochat<sup>17</sup>, C. Romero<sup>17,24</sup>, D. Rouan<sup>6</sup>, M. Samland<sup>7,8</sup>, T. O. B. Schmidt<sup>6,25</sup>, E. Sissa<sup>1</sup>, and F. Wildi<sup>11</sup>

(Affiliations can be found after the references)

Received 16 May 2022 / Accepted 24 June 2022

## ABSTRACT

**Aims.** In this work, we aim to constrain the masses and separations of potential substellar companions to five accelerating stars (HIP 1481, HIP 88399, HIP 96334, HIP 30314, and HIP 116063) using multiple data sets acquired with different techniques.

**Methods.** Our targets were originally observed as part of the SPHERE/SHINE survey, and radial velocity (RV) archive data were also available for four of the five objects. No companions were originally detected in any of these data sets, but the presence of significant proper motion anomalies (PMas) for all the stars strongly suggested the presence of a companion. Combining the information from the PMas with the limits derived from the RV and SPHERE data, we were able to put constraints on the characteristics of the unseen companions.

**Results.** Our analysis led to relatively strong constraints for both HIP 1481 and HIP 88399, narrowing down the companion masses to  $2\text{--}5 M_{\text{Jup}}$  and  $3\text{--}5 M_{\text{Jup}}$  and separations within  $2\text{--}15$  au and  $3\text{--}9$  au, respectively. Because of the large age uncertainties for HIP 96334, the poor observing conditions for the SPHERE epochs of HIP 30314, and the lack of RV data for HIP 116063, the results for these targets were not as well defined, but we were still able to constrain the properties of the putative companions within a reasonable confidence level.

**Conclusions.** For all five targets, our analysis reveals that the companions responsible for the PMA signal would be well within reach for future instruments planned for the ELT (e.g., MICADO), which would easily achieve the required contrast and angular resolution. Our results therefore represent yet another confirmation of the power of multi-technique approaches for both the discovery and characterisation of planetary systems.

**Key words.** instrumentation: spectrographs – methods: data analysis – techniques: imaging spectroscopy – planetary systems

## 1. Introduction

In the last decade, the direct imaging (DI) technique has allowed for the detection of a growing number of planetary mass objects orbiting nearby young stars, such as 51 Eri b (Macintosh et al. 2015), HIP 65426 b (Chauvin et al. 2017b), PDS 70 b (Keppler et al. 2018), and PDS 70 c (Haffert et al. 2019). This was made possible in particular thanks to a new generation of high-contrast imagers mainly devoted to this aim, such as the Gemini Planet Imager (GPI; Macintosh et al. 2014), VLT/SPHERE (Beuzit et al. 2019), and CHARIS (Groff et al. 2015). However, even with such sophisticated instruments, direct detection is limited to giant gaseous companions at large separation (more than 10 au) from the host star. Such limitation mainly arises from the challenge of resolving extremely faint sources (with contrast of the order of  $10^{-6}$ ) at relatively close angular separations (a physical separation of 10 au corresponds to  $0.2''$  for a star at a distance of 50 pc).

In addition, recent studies point out the relative paucity of giant planets (masses larger than  $1 M_{\text{Jup}}$ ) at large separations (Nielsen et al. 2019; Vigan et al. 2021), which, combined with the increasing planetary occurrence rate between 0.1 and 1 au obtained through radial velocity (RV) surveys (see e.g., Fulton et al. 2021), implies that the expected peak for the distribution of giant planets should reside between 1 and 10 au (e.g., Meyer et al. 2018).

While the bulk of the giant planet population therefore appears to be out of reach from current direct imaging surveys, it will likely be the main focus for the future instrumentation of the under-construction extremely large telescopes (ELT; see e.g., Perrot et al. 2018). There are, however, ways to push the discovery space of the current facilities toward the peak of the giant planet population and enhance our comprehension of the formation process of such objects. Concentrating on the nearest stars is an obvious solution, but it is also possible to continue focused programs concentrating efforts on stars that have a higher probability of hosting detectable companions. So far, the most successful selection methods for such programs have been those based on proper motion anomalies (PMas or accelerations; see e.g., Brandt 2018; Kervella et al. 2019) defined as the difference between the short-term and the long-term proper

<sup>★</sup> Based on observations made with European Southern Observatory (ESO) telescopes at the Paranal Observatory in Chile under program IDs 095.C-0298(A), 095.C-0298(B), 096.C-0241(A), 096.C-0241(G), 097.C-0865(A), 097.C-0865(D), 1100.C-0481(F), 1100.C-0481(N), and 1100.C-0481(P).

**Table 1.** Main characteristics of the target stars.

ID	Age <sub>min</sub> <sup>max</sup>	Mass	Sp type	Kmag	Parallax	Proper motion		PMa (HIP-eDR3)		$\Delta v_{\text{tan}}$ (HIP-eDR3)		RUWE	S/N <sub>PMa</sub>
	(Myrs)	( $M_{\odot}$ )			(mas)	(RA: mas yr <sup>-1</sup> )	(Dec: mas yr <sup>-1</sup> )	(RA: mas)	(Dec: mas)	(m s <sup>-1</sup> )	(PA: deg)		
HIP 1481	45 <sub>35</sub> <sup>50</sup>	1.16	F8V	6.15	23.36 ± 0.02	90.05 ± 0.02	-59.21 ± 0.02	-0.10 ± 0.02	0.04 ± 0.02	22.13 ± 6.40	290.07 ± 12.07	0.994	3.46
HIP 30314	149 <sub>100</sub> <sup>180</sup>	1.11	G1V	5.05	41.89 ± 0.01	-11.43 ± 0.02	64.68 ± 0.02	-0.04 ± 0.02	0.10 ± 0.02	12.52 ± 3.51	336.98 ± 11.05	0.874	3.57
HIP 88399	24 <sub>19</sub> <sup>29</sup>	1.29	F6V	5.91	20.29 ± 0.02	2.33 ± 0.02	-86.23 ± 0.02	0.11 ± 0.03	-0.09 ± 0.02	32.66 ± 8.21	130.94 ± 10.17	1.093	3.98
HIP 96334	150 <sub>70</sub> <sup>220</sup>	1.00	G3V	6.3	26.20 ± 0.02	-4.04 ± 0.01	-176.05 ± 0.02	0.04 ± 0.02	0.13 ± 0.02	25.13 ± 5.43	14.63 ± 7.53	0.995	4.63
HIP 116063	300 <sub>200</sub> <sup>500</sup>	0.80	G1V	5.65	33.05 ± 0.02	183.28 ± 0.02	-122.68 ± 0.02	-0.07 ± 0.03	0.09 ± 0.03	16.54 ± 5.45	324.67 ± 12.73	1.107	3.04

**Notes.** Individual references for the stellar ages (expressed as Age<sub>min</sub><sup>max</sup>) and masses are provided in Sect. 2. Parallax and proper motion values are from eDR3, from which we also show the RUWE. The values of the PMa, PMa S/N, and tangential velocity ( $\Delta v_{\text{tan}}$ ) with the corresponding position angle are from Kervella et al. (2022).

motions measured for a star. While in the past these trends have only been used to select targets for binary star searches, the precision on the proper motion measurements achieved by *Gaia* (Gaia Collaboration 2016) now allows us to push towards signals pointing to much smaller companions, down to the substellar and even planetary regimes.

Several groups (see e.g., Kervella et al. 2019, 2022; Brandt 2018, 2021) have recently shared PMa catalogues, including the Hipparcos and *Gaia* DR2/eDR3 proper motions, as well as a *Gaia*-HIPPARCOS scaled positional differences, placing all proper motions at the epochs of *Gaia* DR2 and eDR3, respectively, with recalibrated uncertainties for hundreds of thousands of stars. For our work, we chose to use the catalog from Kervella et al. (2022), and, following their approach, we define stars with a PMa signal-to noise (S/N) larger than 3 as accelerating. As shown by several recent results, accelerating stars have a high probability of hosting companions ranging from low-mass stars to substellar companions, including objects close to planetary mass (see e.g., Bonavita et al. 2022; Currie et al. 2020; Steiger et al. 2021; Chilcote et al. 2021). Even in case of non-detection, the combination of DI data and information concerning the PMas can be used to put constraints on the nature of the possible unseen companions causing the acceleration. In addition, the availability of radial velocity data provides additional information on closer companions. For example, this approach was used by Mesa et al. (2021) to study the disk-hosting star HD 107146, leading to the conclusion that the measured PMa is due to the presence of a companion with a mass of 2–5  $M_{\text{Jup}}$  at a separation of 2–7 au. Results like this one show how such an analysis is therefore crucial to understanding the structure of planetary systems around these stars and can also be used to define a sample of optimal targets for future observations with ELT instruments.

In this paper, we present the results of our analysis for five stars with strong accelerations pointing to the presence of a low-mass companion and for which DI observations were available from SHINE (Chauvin et al. 2017a; Desidera et al. 2021; Langlois et al. 2021; Vigan et al. 2021). While no companion was retrieved from the SHINE observations, they have been used to constrain their presence at separation between 2 and 10 au also using mass limits from archive RV data. A detailed description of each of our targets is provided in Sect. 2, while Sect. 3 presents the various data sets used for our analysis. Our results are presented in Sect. 4 and discussed in Sect. 5. Finally, Sect. 6 provides some concluding remarks.

## 2. Sample selection

The starting point for the target selection was the catalog by Kervella et al. (2022), which lists the PMa value, defined as

the difference in proper motion between HIPPARCOS and *Gaia* eDR3 (Gaia Collaboration 2021), for ~11000 HIPPARCOS stars. From a initial list of targets with PMas with a S/N higher than three, we selected the objects with renormalised unit weight error (RUWE; for a more detailed definition and description of its use see Lindegren et al. 2021) higher than 1.4, to avoid the effects of possible degradation of the astrometric parameters. Moreover, a large value of the RUWE parameter is often caused by stellar binarity as discussed in Kervella et al. (2022). We then restricted our sample to stars within 50 parsecs in order to make sure possible companions responsible for the PMa would be accessible with direct imaging. The final list of 498 targets was then cross-correlated with the list of targets observed during the SHINE survey (Desidera et al. 2021; Langlois et al. 2021). After the exclusion of objects for which the presence of a bound stellar companion was known and able to explain the PMa signal, we were left with five targets: HIP 1481, HIP 88399, HIP 96334, HIP 30314, and HIP 116063. Their main characteristics are summarized in Table 1 and described in detail in the following sections.

### 2.1. HIP 1481

HIP 1481 (HD 1466) is an F8 star (Torres et al. 2006) with a mass of 1.16  $M_{\odot}$  (Desidera et al. 2021), located at a distance of  $42.82 \pm 0.03$  pc from the Sun (Gaia Collaboration 2021). It has been recognised as a member of the Tucana-Horologium moving group (Bell et al. 2015). From this membership, Desidera et al. (2021) deduced an age of  $45^{+5}_{-10}$  Myr.

The presence of a debris disk around HIP 1481 was inferred by Chen et al. (2014) using Spitzer observations. They modeled the SED with a double black body with temperatures of 97 and 374 K, suggesting a double-belt structure of the disk. Using these results, Lazzoni et al. (2018) found a radius of 0.7 au for the inner belt and a radius of ~52 au for the outer belt, with a gap between the two belts of around 40 au. Using dynamical models they then concluded that to explain this disk configuration the presence of at least a planet less massive than 3  $M_{\text{Jup}}$  and with high eccentricity was required.

The PMa retrieved from Kervella et al. (2022) has a S/N of 3.46, making the presence of a companion very likely. They estimated a mass of 3.20  $M_{\text{Jup}}$  for a companion on a 3 au orbit and of 2.55  $M_{\text{Jup}}$  for a companion on a 10 au orbit.

### 2.2. HIP 30314

HIP 30314 (HD 45270) is a G1 star (Torres et al. 2006) with a mass of 1.11  $M_{\odot}$  (Desidera et al. 2021), located at a distance of  $23.87 \pm 0.01$  pc. It is part of the AB Dor association (Zuckerman et al. 2011; Gagné et al. 2018) and it has an estimated age of

**Table 2.** List and main characteristics of the SPHERE observations used for this work.

Target	Date	Obs. mode	Coronagraph	DIMM seeing	$\tau_0$	wind speed	Field rotation	DIT	Total exp.
HIP 1481	26 Oct. 2015	IRDIFS	N_ALC_YJH_S	1.08''	1.4 ms	1.77 m s <sup>-1</sup>	25.1°	64 s	4096 s
HIP 1481	18 Sep. 2016	IRDIFS	N_ALC_YJH_S	0.80''	5.0 ms	9.95 m s <sup>-1</sup>	25.1°	64 s	5120 s
HIP 30314	16 Jan. 2016	IRDIFS	N_ALC_YJH_S	1.73''	1.5 ms	10.93 m s <sup>-1</sup>	27.2°	64 s	4096 s
HIP 88399	10 May 2015	IRDIFS	N_ALC_YJH_S	1.86''	1.2 ms	2.63 m s <sup>-1</sup>	34.5°	64 s	3584 s
HIP 88399	1 Jun. 2015	IRDIFS	N_ALC_YJH_S	1.25''	1.1 ms	2.48 m s <sup>-1</sup>	34.1°	64 s	4096 s
HIP 88399	17 Apr. 2016	IRDIFS	N_ALC_YJH_S	1.58''	1.5 ms	14.73 m s <sup>-1</sup>	37.2°	64 s	3776 s
HIP 88399	11 Apr. 2018	IRDIFS	N_ALC_YJH_S	0.52''	5.6 ms	7.45 m s <sup>-1</sup>	32.0°	96 s	3840 s
HIP 88399	7 Sep. 2019	IRDIFS	N_ALC_YJH_S	1.14''	1.9 ms	12.75 m s <sup>-1</sup>	40.7°	96 s	4896 s
HIP 96334	10 May 2019	IRDIFS	N_ALC_YJH_S	0.47''	4.6 ms	8.73 m s <sup>-1</sup>	32.8°	96 s	6144 s
HIP 116063	7 Sep. 2019	IRDIFS	N_ALC_YJH_S	2.06''	1.5 ms	18.23 m s <sup>-1</sup>	31.6°	64 s	4032 s

149<sup>+31</sup><sub>-49</sub> Myr (Desidera et al. 2021). The S/N of the PMa for HIP 30314 is 3.57, and Kervella et al. (2022) estimated a mass of 1.66  $M_{\text{Jup}}$  for an object orbiting 3 au from the star and of 1.40  $M_{\text{Jup}}$  for a companion orbiting 10 au from the star.

### 2.3. HIP 88399

HIP 88399 (HD 164249) is an F6 star (Torres et al. 2006) with a mass of 1.29  $M_{\odot}$  (Zúñiga-Fernández et al. 2021) located at a distance of  $49.30 \pm 0.06$  pc from the Sun (Gaia Collaboration 2021). It is part of the  $\beta$  Pictoris moving group (e.g., Messina et al. 2017) and has an estimated age of  $24 \pm 5$  Myr (Desidera et al. 2021). HIP 88399 has a known companion, HD 164249 B, an M2 star with an estimated mass of 0.54  $M_{\odot}$  (Zúñiga-Fernández et al. 2021), and a separation of  $\sim 6.5''$  corresponding to  $\sim 323$  au at the distance of the system (Pawellek et al. 2021). IR excess was detected using both WISE (Wright et al. 2010), *Spitzer* (Chen et al. 2014) and Herschel (Eiroa et al. 2013) data, hinting at the presence of a debris disk. The disk was finally resolved through ALMA observations by Pawellek et al. (2021), who estimated a radius of 63 au for the disk and an inclination lower than 49°. HIP 88399 has a PMa S/N of 3.98, providing a strong indication of the presence of a substellar object at short separation from the star or of a larger mass companion at larger separation.

### 2.4. HIP 96334

HIP 96334 (HD 183414) is a G3 star (Torres et al. 2006) with a mass of 1.00  $M_{\odot}$  (Vigan et al. 2017) at a distance of  $38.16 \pm 0.03$  pc from the Sun (Gaia Collaboration 2021). It is not part of any known young moving group. Its age has been evaluated as  $150^{+70}_{-80}$  Myr (Vigan et al. 2017). This star was a target both for direct imaging (see e.g., Chauvin et al. 2010; Nielsen et al. 2019) and RV (see e.g., Grandjean et al. 2020) with no detection of a low-mass stellar or substellar companion. Kervella et al. (2022) lists a PMa S/N of 4.63, which makes the presence of a companion very probable.

### 2.5. HIP 116063

HIP 116063 (HD 221231) is a G1 star (Torres et al. 2006) with a mass of 0.8  $M_{\odot}$  (Vigan et al. 2017) located at a distance of  $30.25 \pm 0.02$  pc from the Sun (Gaia Collaboration 2021). Its age is  $300^{+200}_{-100}$  Myr (Desidera et al. 2015). A wide companion for this star is known (TYC-9339-2158-1; Desidera et al. 2015), but its large separation ( $36.3''$  corresponding to more than 1100 au) and mass (0.80  $M_{\odot}$ ) are not compatible with the detected PMa. The

value of the PMa S/N for HIP 116063 is 3.04, which is just above the threshold suggesting the presence of a possible companion.

## 3. Observations and data reduction

### 3.1. Direct imaging data

All our objects were observed as part of the SPHERE/SHINE program. Table 2 shows the main characteristics of the observations, all performed using the IRDIFS SPHERE observing mode, which uses both IFS (Claudi et al. 2008) operating in  $Y$  and  $J$  spectral bands between 0.95 and 1.35  $\mu\text{m}$  on a  $1.7'' \times 1.7''$  field of view (FOV) and IRDIS (Dohlen et al. 2008) covering in the  $H$  spectral band using the  $H23$  filter pair (wavelength  $H2 = 1.593 \mu\text{m}$ ; wavelength  $H3 = 1.667 \mu\text{m}$ ; Vigan et al. 2010) on a circular FOV of  $\sim 5''$ . All the observations were performed exploiting the SPHERE adaptive optics system SAXO (Fusco et al. 2006).

At all epochs, we acquired frames with satellite spots that are symmetrical with respect to the central star just before and just after the science sequence. We used these to precisely define the position of the star behind the coronagraph (Langlois et al. 2013). To obtain photometric calibration, we also observed each star without the coronagraph, using an appropriate neutral density filter to avoid the saturation of the detectors.

As detailed in Table 2, multiple epochs were available for HIP 1481 and HIP 88399. Unfortunately, only one the five data sets available for HIP 88399 was taken in good enough weather conditions (11 Apr. 2018). The same is true for HIP 1481, for which the conditions were significantly better on the second night (18 Sep. 2016). Therefore, we only use these data sets for our analysis of these two objects.

All data were reduced using the SPHERE data center (Delorme et al. 2017). The first step was to apply the appropriate calibrations following the data reduction and handling pipeline (DRH; Pavlov et al. 2008). For IRDIS, the required calibrations include the creation of the master dark and master flat-field frames and the definition of the star center. For IFS, it was also necessary to define the position of each spectra on the detector as well as the wavelength calibration and the application of the instrumental flat that takes into account the different response of each lenslet of the IFS array. To the reduced data, we then applied speckle subtraction using both angular differential imaging (ADI; Marois et al. 2006) and spectral differential imaging (SDI; Racine et al. 1999). These methods were implemented using both the principal components analysis (PCA; Soummer et al. 2012) and the TLOCI (Marois et al. 2014) algorithms. They are applied to the SPHERE case as described in Zurlo et al. (2014) and in Mesa et al. (2015), and they are



**Table 3.** Astrometry for the four candidate companions in the IRDIS FOV of HIP 88399 retrieved from the first and last SPHERE data sets.

cc	Obs. date	Sep. RA (mas)	Sep. Dec (mas)	Total sep. (mas)	PA (°)
1	10 May 2015	$-661.50 \pm 6.13$	$-1115.98 \pm 6.13$	$1297.30 \pm 8.66$	$210.7 \pm 0.1$
1	7 Sep. 2019	$-649.25 \pm 6.13$	$-758.28 \pm 6.13$	$998.25 \pm 8.66$	$220.6 \pm 0.1$
2	10 May 2015	$2130.28 \pm 6.13$	$-2757.48 \pm 6.13$	$3484.50 \pm 8.66$	$142.3 \pm 0.1$
2	7 Sep. 2019	$2142.53 \pm 6.13$	$-2418.15 \pm 6.13$	$3230.77 \pm 8.66$	$138.5 \pm 0.1$
3	10 May 2015	$-3173.98 \pm 6.13$	$-2878.75 \pm 6.13$	$4285.01 \pm 8.66$	$227.8 \pm 0.1$
3	7 Sep. 2019	$-3150.70 \pm 6.13$	$-2527.18 \pm 6.13$	$4039.00 \pm 8.66$	$231.3 \pm 0.1$
4	10 May 2015	$-3197.25 \pm 6.13$	$4120.90 \pm 6.13$	$5125.77 \pm 8.66$	$322.2 \pm 0.1$
4	7 Sep. 2019	$-3186.23 \pm 6.13$	$4477.38 \pm 6.13$	$5495.35 \pm 8.66$	$324.6 \pm 0.1$

currently implemented through the SpeCal pipeline (Galicher et al. 2018).

### 3.2. RV data

Radial velocity data, acquired with the HARPS spectrograph, were available from Trifonov et al. (2020) for HIP 1481 (24 data points), HIP 30314 (27 data points), HIP 88399 (38 data points), and HIP 96334 (71 data points). Unfortunately, no RV data, taken with HARPS or any other RV instrument, were available for HIP 116063. The retrieved RV data were used to obtain mass limits for possible companions at low separations from the host stars using the Exoplanets Detection Map Calculator (EXO-DMC; Bonavita 2020) and following the method described in Mesa et al. (2021).

### 3.3. PMa data

All the PMa data used for this work were obtained from the catalog by Kervella et al. (2022). Following their approach, we considered all the targets with a PMa S/N larger than 3 as probable companion hosting stars. Using the method described in Kervella et al. (2019), we were able to estimate the mass of the companions compatible with the PMa signal as a function of the separation from the host star (see their Eq. (1)). The resulting limits are shown in Sect. 5.2 (blue solid lines). It is important to note that the mass is calculated assuming a circular orbit while a statistical distribution for its inclination is taken into account following the method devised in Kervella et al. (2019). The values obtained should therefore be regarded as a minimum mass for the object causing the PMa signal. Moreover, the possible positions of the companion generating the PMa signal can be further limited using the position angle (PA) of the velocity anomaly vector  $\Delta v_{\text{tan}}$ , as shown by Bonavita et al. (2022). We will discuss the resulting constraints in Sect. 6.

## 4. Results

### 4.1. Candidate companions

We first inspected the reduced DI data to look for candidate companions that could explain the PMa signal. In the cases of HIP 1481, HIP 30314, and HIP 116063, we did not find any candidate within the IFS or IRDIS FOV.

Four candidates were identified in the IRDIS images of HIP 88399, all at separations larger than  $1''$  and therefore not included in the IFS images. Figure 1 shows the IRDIS image of HIP 88399, acquired on 11 Apr. 2018 (the night with the best weather conditions), with the candidates highlighted in white. The bright source at the extreme east of the IRDIS image is the known stellar companion: HD 164249 B. Given its position, it

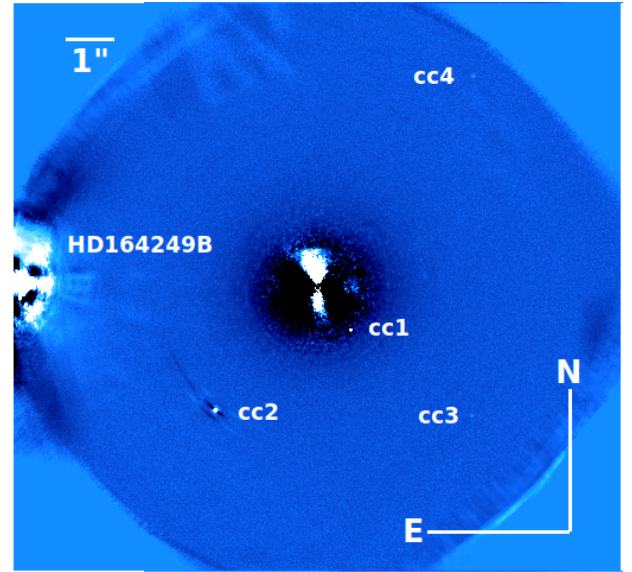


**Fig. 1.** Final IRDIS image for HIP 88399 obtained from data taken on 11 Apr. 2018. The four candidate companions are marked as cc1, cc2, cc3, and cc4, respectively. The known stellar companion HD 164249 B is partially visible at the eastern edge of the image.

was not possible to extract any astrometric value for this star as its PSF was not within the IRDIS FoV.

Table 3 includes the values of the relative astrometry of each candidate, obtained for the first and last epochs available (10 May 2015 and 7 Sep. 2019), which were used to check for common proper motion. For all the data, we adopted a rather conservative error bar of half of the IRDIS pixel scale. In Fig. 2, we compare these astrometric values with the relative astrometric position of a background object that is indicated by a blue cross. This position can be easily calculated starting from the known proper motion and the parallax of the host star and from the dates of the observing epochs. A background object with no proper motion would be expected at the separation and PA indicated by the blue cross at the epoch of the second observation (indicated by the filled blue circle). Because a background object displays some proper motion, perfect correspondence is not expected. For the Fig. 2 plots, the filled blue circle is very near the expected position for a background object. Hence, we disprove the assertion that these objects are gravitationally bound to the host star. In this latter case, we would expect the position of the filled blue circle to be almost coincident with the relative position of the first observation (filled red circle). In this latter, case the only source of movement should be the orbital motion of the companion, which, because of the large separation of such objects,

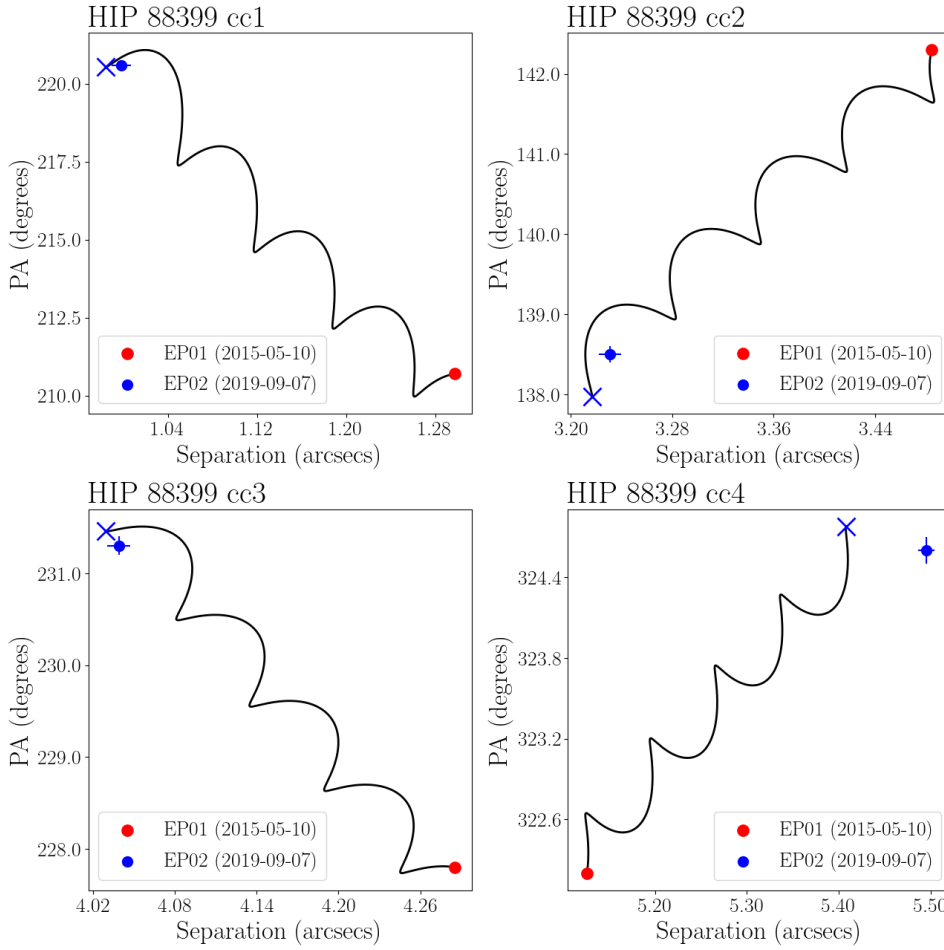


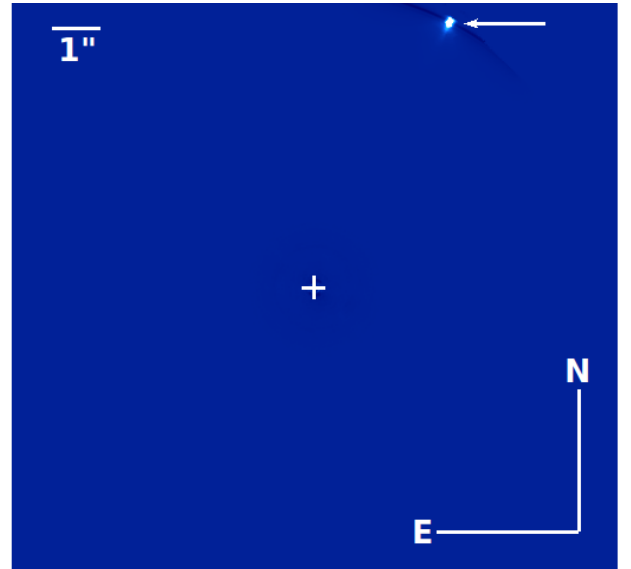
**Fig. 2.** Common proper motion analysis of all the candidate companions identified for HIP 88399. In all panels, the solid black line shows the motion of a background object relative to the target, based on the eDR3 parallax and proper motion of the primary over the same time frame. The filled circles show the measured separation and position angle of the companions at the first (red) and second (blue) epochs. The blue cross indicates the expected position of a background object at the second epoch.

is expected to be very small. Some examples showing these plots for gravitationally bound objects could be found, for example, in Fig. 4 of Bonavita et al. (2022). We therefore concluded that none of these objects could be the cause of the measured PMa.

One candidate companion was also identified at the edge of the IRDIS FOV for HIP 96334, as shown in Fig. 3. Although only one SPHERE epoch was available for this target, we were able to perform a common proper motion analysis (the results of which are shown in Fig. 4) using NaCo data available in the ESO archive (Program ID: 079.C-0908(A); PI: B. Zuckerman) taken on 9 Jun. 2007, where the candidate was also visible. The astrometry values for the two epochs are listed in Table 4. Following the same approach described above for HIP 88399, we were able to confirm that the candidate is a background source, a conclusion strengthened by the detection of the companion in eDR3, where it is listed with a parallax that is inconsistent with that of HIP 96334.

#### 4.2. Contrast limits

For each target, we calculated the contrast limits for both IFS and IRDIS, using the method described in Mesa et al. (2015). The self-subtraction due to the speckle subtraction method was estimated including simulated objects at different separations from the star and consequently corrected. Finally, the results were corrected taking into account the effect of the small sample statistics as defined by Mawet et al. (2014). The resulting contrast limits are shown in Fig. 5. We note that for HIP 1481 and

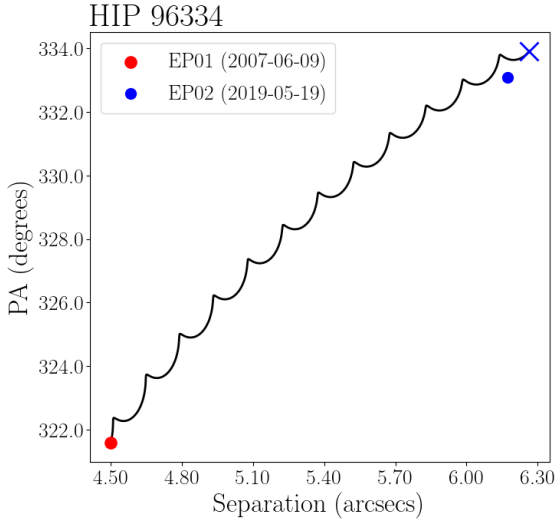


**Fig. 3.** Final IRDIS image for HIP 96334. The candidate companion is indicated by the white arrow in the upper part of the image. The position of the star behind the coronagraph is indicated by a white cross.

HIP 88399, for which more than one data set was available, we choose to show only the limits obtained using the data taken on the nights with the best weather conditions (18 Sep. 2016 and 11 Apr. 2018, respectively).

**Table 4.** Astrometry of the candidate companion to HIP 96334 for the two epochs considered in this work, obtained from NACO and SPHERE observations.

Obs. date	Instrument	Pixel scale (mas)	Sep. RA (mas)	Sep. Dec (mas)	Total sep. (mas)	PA (°)
9 Jun. 2007	NACO	27.15	$-2793.74 \pm 13.58$	$3529.50 \pm 13.58$	$4501.37 \pm 19.20$	$321.6 \pm 0.2$
19 May 2019	SPHERE/IRDIS	12.25	$-2793.00 \pm 6.13$	$5503.93 \pm 6.13$	$6172.04 \pm 8.66$	$333.1 \pm 0.1$

**Fig. 4.** Common proper motion analysis for candidate companion to HIP 96334. The solid black line shows the motion of a background object relative to the target, based on the eDR3 parallax and proper motion of the primary over the same time frame. The filled circles show the measured separation and position angle of the companions at the first (red) and second (blue) epochs. The blue cross indicates the expected position of a background object at the second epoch.

#### 4.3. Mass limits and comparison with PMa results

The contrast limits shown in Fig. 5 were converted into mass limits using the AMES-COND evolutionary models (Allard et al. 2003) and adopting the stellar ages listed in Table 1. We then compared these mass limits with those obtained using the RV data (see Sect. 3.2) as well as with the estimates of the mass of the companion responsible for the PMa signal calculated as described in Sect. 3.3. This allowed us to put further constraints on the mass and the separation of the possible unseen companions. At this point, we again stress that the mass limits calculated in Sect. 3.3 assume circular orbits and therefore only provide an indication of the order of magnitude for the mass of the companion generating the PMa signal, rather than an exact value. The results of the comparison are shown in Fig. 6, where the limits from the PMa are shown as solid blue lines, the RV limits as violet lines, and the DI limits as green, orange, and red solid lines, depending on the age used for the conversion (minimum, adopted, and maximum values, respectively). For HIP 1481 (top left panel) and HIP 88399 (center left panel), we also include black dashed lines marking the expected positions of the known debris disks.

## 5. Discussion

The procedure described in the previous sections allowed us to determine different constraints on mass and separations for each of the targets considered in this work. The most promising results

were obtained for HIP 1481. As can be seen in the upper left panel of Fig. 6, the DI mass limits exclude the presence of the companion responsible for the PMa signal at separations larger than  $\sim 15$  au, while at short separations of less than 2–3 au the RV mass limits exclude the presence of this companion. The possible values of the mass of this object range from 2–5  $M_{\text{Jup}}$  with the higher masses possible only at the lower allowed separations. The probability of a companion at separations smaller than  $\sim 1$  au and at separations of 40–60 au is further diminished by the presence of the inner and the outer belt of the debris disk found around this star.

The constraints that we can obtain for the case of HIP 30314 are not as strong (see the upper right panel of Fig. 6). Due to the poor weather conditions during the SPHERE observation (see Table 2) and the older age of this system, the DI limits are worse than those achieved for HIP 1481, especially at short separations (see red and orange solid lines in Fig. 5), and they can only exclude companions at separations larger than  $\sim 30$  au. The limits produced using the RV are also higher than in the case of HIP 1481, thus providing much less stringent constraints at separations smaller than 1 au. The possible mass values range between  $\sim 1 M_{\text{Jup}}$  and 5  $M_{\text{Jup}}$  at separations larger than 2 au, while they could be as large as 10  $M_{\text{Jup}}$  at separations lower than 2 au.

The limits on the separation for HIP 88399 from the DI data allow us to exclude the presence of the companion causing the PMa signal at separations larger than 7–9 au (depending on the chosen value of the age). On the other hand, the mass limits from the RV data are very low and they seem to exclude separations lower than  $\sim 3$  au for the companion generating the PMa signal. The mass of the possible companion ranges between 3 and 5  $M_{\text{Jup}}$  with possible higher masses (up to 8–9  $M_{\text{Jup}}$ ) at the lower end of the separations range. As discussed in Sect. 2, this star has a companion with an estimated mass of  $0.54 M_{\odot}$  (corresponding to  $\sim 566 M_{\text{Jup}}$ ) and a separation of  $\sim 323$  au. Looking at the PMa limit in Fig. 6 (blue curve) we can see that at the separation of this companion, the mass requested to explain the PMa signal is of  $1547.4 M_{\text{Jup}}$  with a lower limit of  $856.3 M_{\text{Jup}}$ , thus it is well above the estimated mass for the companion. This is also true when considering higher masses found in literature: for example, the value of  $0.6 M_{\odot}$  corresponding to  $\sim 628.6 M_{\text{Jup}}$  (Desidera et al. 2021). Moreover, the separation used here for this companion is the projected one. The real separation of this object could then be even larger, making the difference between its mass and the one required to explain the PMa signal more evident<sup>1</sup>. As further confirmation, we also note that the PA of the companion ( $\sim 90^\circ$ ) is not compatible with that derived by Kervella et al. (2022) from the PMa ( $130.94^\circ \pm 10.17^\circ$ ), with a difference larger than  $3\sigma$  between the two values. While from each single value listed above it is difficult to draw a conclusion because of their large uncertainties, the combination of all these indications strongly hints toward the exclusion of the known

<sup>1</sup> Once again, we note that the determination of the mass obtained in this way is valid under the assumption of circular orbits. Eccentric orbits could broaden the mass distribution at the separation of the companion.

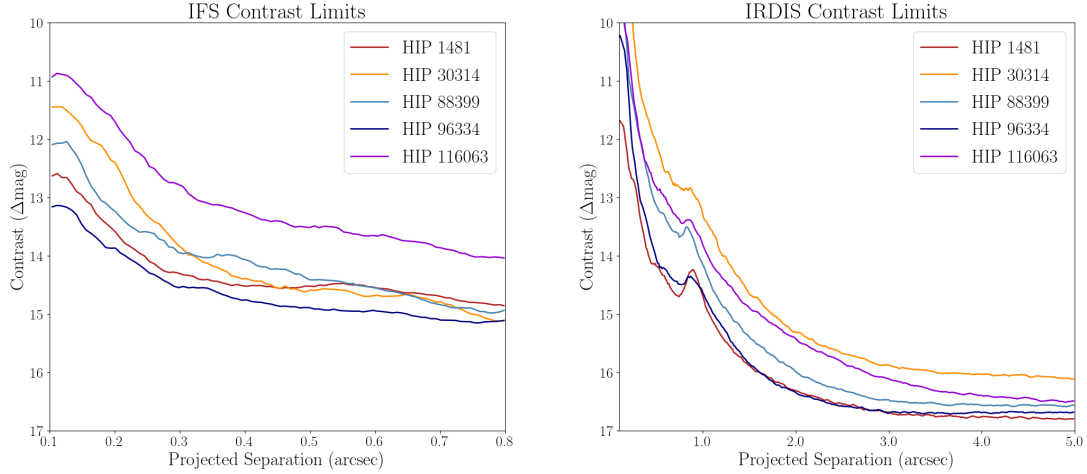


**Fig. 5.** Contrast limits, expressed in magnitude, obtained for all of our targets for IFS (*left panel*) and IRDIS (*right panel*) images. In case of multiple epochs, the plotted limit is the one corresponding to the epoch with the best weather conditions. Specifically, the data taken on 18 Sep. 2016 were used for HIP 1481 (red line), and those taken on 11 Apr. 2018 were used for HIP 88399 (light blue line).

companion being responsible for the PMa signal. In any case, further data, both from astrometry and DI, are still needed to further clarify the situation.

The large errors concerning the age of HIP 96334 lead to very different mass limits from the DI images, and this has quite a large impact on the constraints we could put on the nature of the PMa companion. In fact, when considering an age of 70 Myr (green solid line in the center right panel of Fig. 6), DI data exclude companions at separations larger than  $\sim 7$  au. Instead, when considering the much older ages of 150 and 200 Myr (orange and red lines in the center right panel of Fig. 6), we were only able to exclude possible companions at separations larger than  $\sim 20$  au. On the other hand, mass limits from the RV allow us to exclude any possible companions at separations lower than  $\sim 3$  au. From the mass point of view, an age of 70 Myr would allow for a companion of  $3\text{--}4 M_{\text{Jup}}$ , while the older ages would allow masses as high as  $5\text{--}7 M_{\text{Jup}}$ .

The lack of RV data limited our ability to put constraints on companions within 1 au of HIP 116063, where we cannot exclude masses as large as  $\sim 100 M_{\text{Jup}}$ . At larger separations, the bad quality of the DI data and the relatively high age of the system only allowed us to exclude companions at separation larger than 30 au with masses that can be as high as  $10 M_{\text{Jup}}$ .

### 5.1. FORECAST maps

The limits shown in Fig. 6 were derived using the absolute value of the PMa reported in Table 1. However, as mentioned in Sect. 3.3, further constraints can be applied to take advantage of the vectorial nature of the PMa, and in particular of the information on its position angle. We therefore used the tool Finely Optimised Retrieval of Companions of Accelerating STars (FORECAST) tool (for details and other uses see Bonavita et al. 2022) to isolate the region on the plane of the sky where the companion compatible with the PMa should lie, based on the PA values reported in Table 1.

For each target, FORECAST evaluates the position angle of each pixel in the IFS image with respect to the center and then compares it with the PMa position angle (PA<sub>pm</sub>) retrieved from the catalogue by Kervella et al. (2022). The optimal region (shown in blue in Fig. 7) is then identified by the X and Y positions on the image where the position angle is within one sigma from the PA<sub>pm</sub> value, plus or minus an additional quantity that

takes into account the possible orbital motion of a companion at that separation between the SPHERE observation and the *Gaia* observations.

Finally, it also associates a value of the companion mass based on the PMa absolute value with each point of the resulting 2D map, again using the approach from Kervella et al. (2019), similarly to what was done to obtain the PMa limits shown in Fig. 6. Using this information, we could further limit the possible positions of the companion on the IFS FOV at the epoch of the observation. Once again, since no information is available about the eccentricity and inclination of the orbits, this method only provides a rough indication of the position compatible with circular and edge-on orbits. The FORECAST maps can also be used as finding charts to identify the area where to search for possible companions. Figure 7 displays the FORECAST maps obtained for all our targets, considering the IFS FOV. For each panel, the distance bar corresponds to a separation of  $0.3''$ , which we then converted to au using the distance of the targets. To take into account the constraints derived from Fig. 6, we highlighted the regions excluded thanks to the RV (purple) and SPHERE limits (orange). Combined with Fig. 6, Fig. 7 therefore provides further visual confirmation that while for HIP 1481 and HIP 88399 our limits are relatively tight, for HIP 30314 and HIP 116063 the allowed position area is much larger.

The HIP 1481 and HIP 88399 systems present similarities with our Solar System as both of them have a solar-type central star with a debris belt at few tens of au (similar to the Kuiper belt) and a very probable Jupiter-mass planet at a separation comparable to that of Jupiter. For these reasons, they could be regarded as young analogs of the Solar System, making their study even more interesting.

### 5.2. Probability of future detection with DI observations

The SPHERE observations for HIP 88399 and HIP 96334 were taken in good observing conditions, so it is unlikely that new observations with such instruments could achieve a substantial improvement in contrast (and in the mass limits). This suggests a low probability of direct companion detection using current high-contrast imagers. The observations for HIP 1481 were instead taken in intermediate conditions (in particular, strong wind; see Table 2). Better observing conditions could improve the contrast and the mass limits for this star, helping



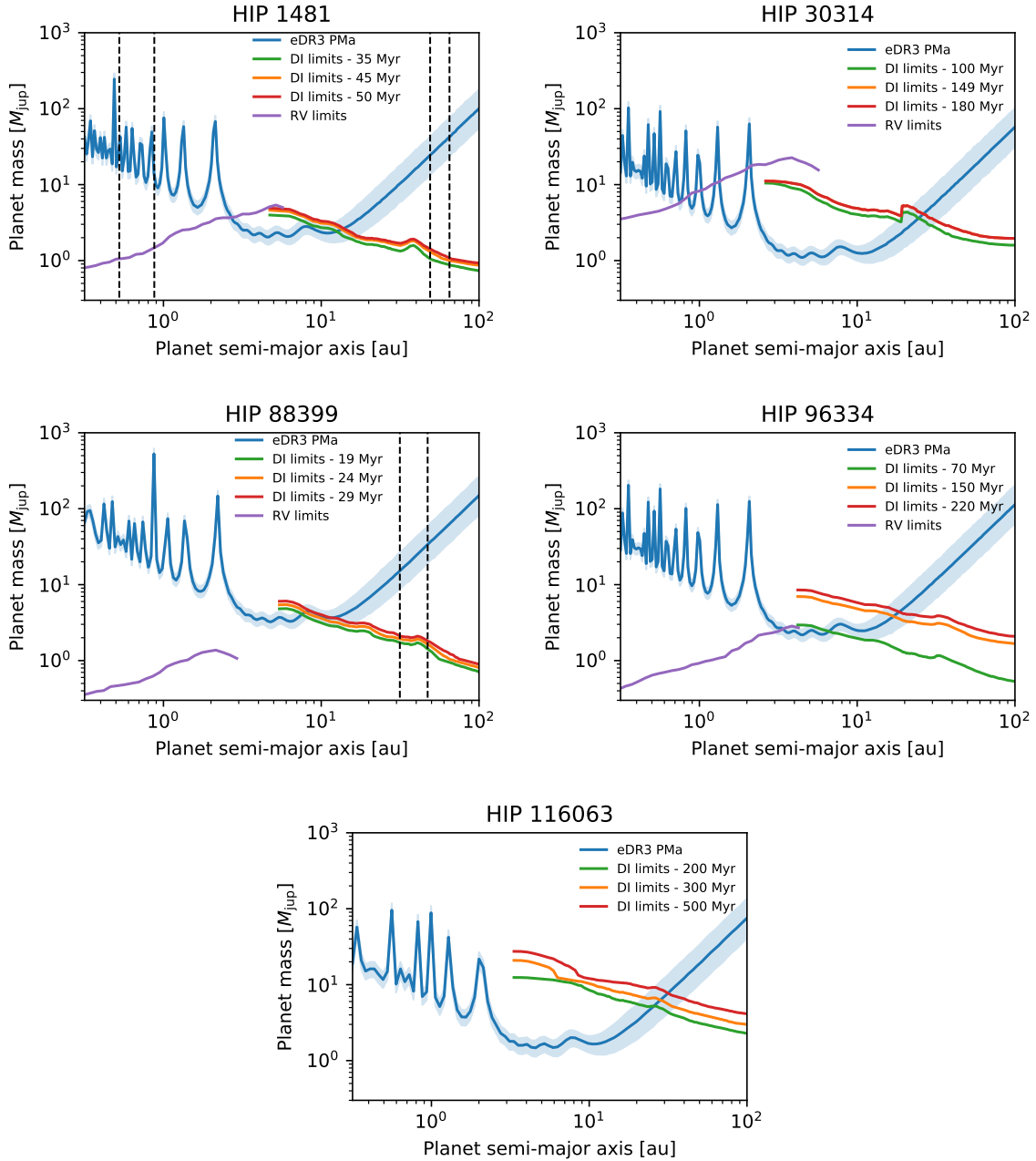


**Fig. 6.** Plots of the mass as function of the separation from the host star of the companion needed to explain the PMA measurement at the *Gaia* eDR3 epoch (blue lines) for HIP 1481 (*top left panel*), HIP 30314 (*top right panel*), HIP 88399 (*center left panel*), HIP 96334 (*center right panel*), and HIP 116063 (*bottom panel*). The blue shaded areas display the  $1\sigma$  confidence interval. The violet lines represent the mass limits from RV data (assuming 95% confidence level). The DI mass limits assuming minimum, expected, and maximum ages are shown by the green, orange, and red lines, respectively. Finally, for HIP 1481 and HIP 88399, we also included the positions of the belts (two in the cases of HIP 1481) composing the debris disk detected around these stars. They are indicated by black dashed lines.

to detect the companion or further constrain its mass and separation. On the other hand, longer observations would not be useful to improve the contrast limits as at large angular separations from the passage at the meridian the rotation of the FOV is low, making a high-contrast method such as ADI less effective. Finally, the observations for HIP 30314 and HIP 116063 were taken in bad weather conditions, limiting the contrast reached for these targets. This leaves some room for improvements in constraining the positions and the mass of the companions with future observations with SPHERE. In any case, the relatively advanced ages (above 100 Myr) for both of them makes the direct detection of the companions very challenging, especially if they reside at separations of less than 10 au.

However, these stars should be ideal targets for future instrumentation at ELT. We note that the contrasts obtained from simulations of the performance of ELT first generation instruments such as MICADO (e.g., [Perrot et al. 2018](#)) would allow the detection for the proposed companions for each separation and mass, as constrained by our analysis. This type of analysis thus proves to be a very powerful tool to select interesting targets for observations with ELT instruments.

## 6. Conclusions

This paper presents a detailed analysis based on the combination of DI, RV, and astrometric data for five stellar systems

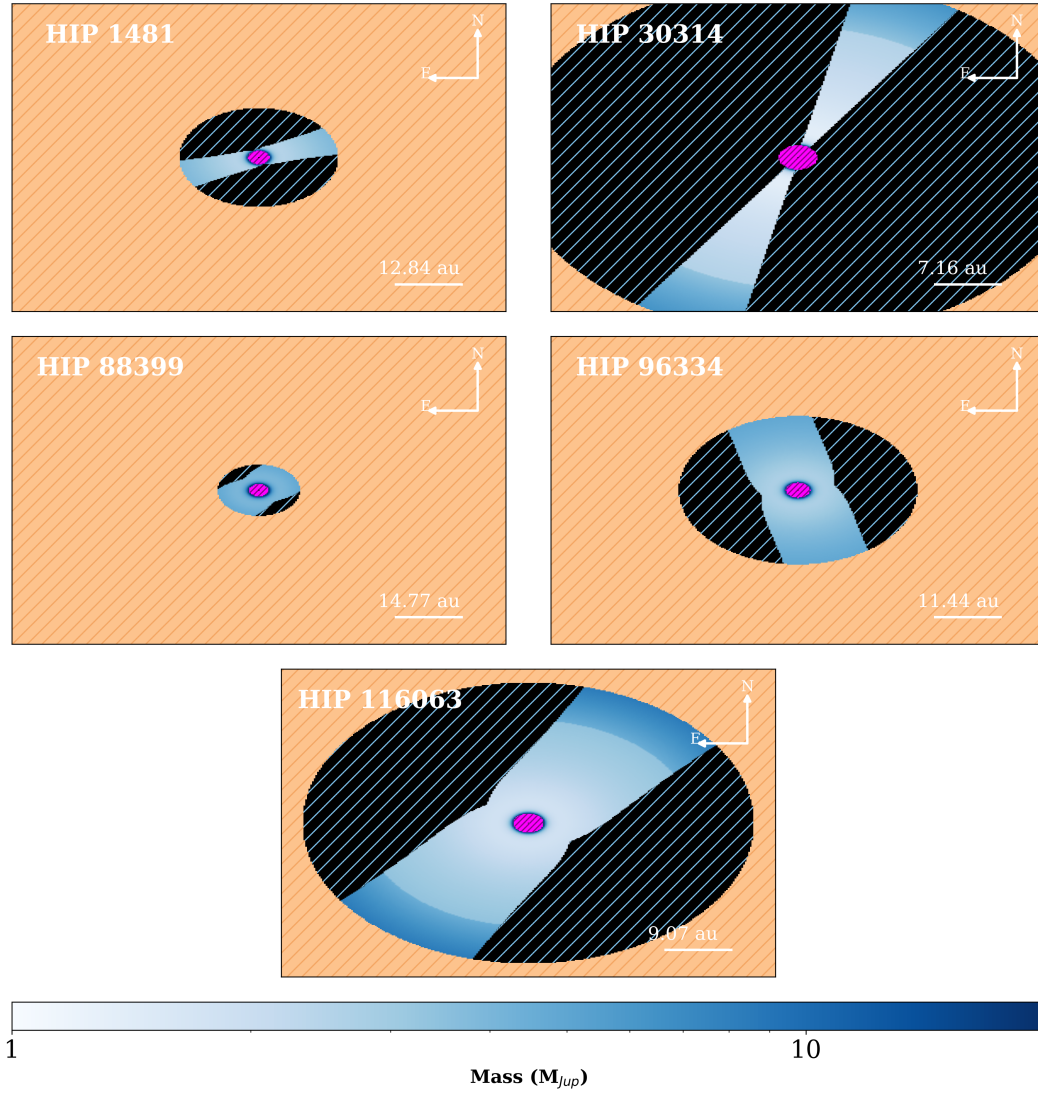


**Fig. 7.** 2D maps obtained with FORECAST (for details see Bonavita et al. 2022) showing the sky area compatible with the PMA reported in Table 1 in blue. The intensity of the blue areas changes according to the dynamical mass (in  $M_{Jup}$ ) responsible for the PMA at a given distance; the same logarithmic scale, shown at the bottom of the figure, was used for all stars. The bar shows the separation corresponding to 0.3'', expressed in au using the distance of each system. The dashed areas show the regions excluded due to incompatibility with the PMA (black) and using the limits from direct imaging (orange) and radial velocity (purple), respectively (see Fig. 6).

showing significant acceleration (PMA) signals, suggesting the presence of planetary companions within a few au. We were able to put constraints on the possible separation and mass of unseen companions on circular orbits for each considered system.

Such constraints were particularly strong for HIP 1481, for which we were able to limit the possible companion separations to 2–15 au and masses of the order of a few  $M_{Jup}$ . Also interesting are the cases of HIP 88399 and HIP 96334, for which similar constraints can be obtained despite the limits imposed by the strong uncertainty on the age. For HIP 88399, although more data are needed for final confirmation, our analysis seems to exclude the known wide companion HD 164249 B as the reason of the PMA signal.

Finally, looser constraints were possible for HIP 30314 and HIP 116063. The bad weather conditions in which the DI observations were taken in both cases and the lack of RV data in the second case strongly limited our capacity to put constraints on both mass and separation. Despite such difficulties, these targets still proved interesting, with a good probability of the presence of a companion at separations between a few au and up to 20–30 au.

While the characteristics of the companions compatible with the PMA strongly limit the feasibility of a detection with current high-contrast instruments (e.g., SPHERE and GPI), they represent ideal targets for observations with ELT-class telescopes, as their proposed masses and separations fit perfectly with the estimated performance of the instruments planned for these facilities.

*Acknowledgements.* This work has made use of the SPHERE Data Center, jointly operated by OSUG/IPAG (Grenoble), PYTHEAS/LAM/CeSAM (Marseille), OCA/Lagrange (Nice) and Observatoire de Paris/LESIA (Paris). This work has made use of data from the European Space Agency (ESA) mission *Gaia* (<https://www.cosmos.esa.int/gaia>), processed by the *Gaia* Data Processing and Analysis Consortium (DPAC, <https://www.cosmos.esa.int/web/gaia/dpac/consortium>). Funding for the DPAC has been provided by national institutions, in particular the institutions participating in the *Gaia* Multilateral Agreement. This research has made use of the SIMBAD database, operated at CDS, Strasbourg, France. This work has been supported by the PRIN-INAF 2019 “Planetary systems at young ages (PLATEA)” and ASI-INAF agreement n.2018-16-HH.0. A.Z. acknowledges support from the CONICYT + PAI/ Convocatoria nacional subvención a la instalación en la academia, convocatoria 2017 + Folio PAI77170087. SPHERE is an instrument designed and built by a consortium consisting of IPAG (Grenoble, France), MPIA

(Heidelberg, Germany), LAM (Marseille, France), LESIA (Paris, France), Laboratoire Lagrange (Nice, France), INAF-Osservatorio di Padova (Italy), Observatoire de Genève (Switzerland), ETH Zurich (Switzerland), NOVA (Netherlands), ONERA (France) and ASTRON (Netherlands), in collaboration with ESO. SPHERE was funded by ESO, with additional contributions from CNRS (France), MPIA (Germany), INAF (Italy), FINES (Switzerland) and NOVA (Netherlands). SPHERE also received funding from the European Commission Sixth and Seventh Framework Programmes as part of the Optical Infrared Coordination Network for Astronomy (OPTICON) under grant number RII3-Ct-2004-001566 for FP6 (2004-2008), grant number 226604 for FP7 (2009-2012) and grant number 312430 for FP7 (2013-2016). For the purpose of open access, the authors have applied a Creative Commons Attribution (CC BY) licence to any Author Accepted Manuscript version arising from this submission.

## References

- Allard, F., Guillot, T., Ludwig, H.-G., et al. 2003, in *Brown Dwarfs*, ed. E. Martín (Berlin: Springer), 211, 325
- Bell, C. P. M., Mamajek, E. E., & Naylor, T. 2015, *MNRAS*, **454**, 593
- Beuzit, J. L., Vigan, A., Mouillet, D., et al. 2019, *A&A*, **631**, A155
- Bonavita, M. 2020, *Astrophysics Source Code Library* [record [ascl:2010.008](#)]
- Bonavita, M., Fontanive, C., Gratton, R., et al. 2022, *MNRAS*, **513**, 5588
- Brandt, T. D. 2018, *ApJS*, **239**, 31
- Brandt, T. D. 2021, *ApJS*, **254**, 42
- Chauvin, G., Lagrange, A. M., Bonavita, M., et al. 2010, *A&A*, **509**, A52
- Chauvin, G., Desidera, S., Lagrange, A. M., et al. 2017a, in *SF2A-2017: Proceedings of the Annual meeting of the French Society of Astronomy and Astrophysics*, eds. C. Reylé, P. Di Matteo, F. Herpin, et al.
- Chauvin, G., Desidera, S., Lagrange, A. M., et al. 2017b, *A&A*, **605**, L9
- Chen, C. H., Mittal, T., Kuchner, M., et al. 2014, *ApJS*, **211**, 25
- Chilcote, J., Tobin, T., Currie, T., et al. 2021, *AJ*, **162**, 251
- Claudi, R. U., Turatto, M., Gratton, R. G., et al. 2008, *SPIE Conf. Ser.*, **7014**, 70143E
- Currie, T., Brandt, T. D., Kuzuhara, M., et al. 2020, *ApJ*, **904**, L25
- Delorme, P., Meunier, N., Albert, D., et al. 2017, in *SF2A-2017: Proceedings of the Annual meeting of the French Society of Astronomy and Astrophysics*, eds. C. Reylé, P. Di Matteo, F. Herpin, et al.
- Desidera, S., Covino, E., Messina, S., et al. 2015, *A&A*, **573**, A126
- Desidera, S., Chauvin, G., Bonavita, M., et al. 2021, *A&A*, **651**, A70
- Dohlen, K., Langlois, M., Saisse, M., et al. 2008, *SPIE Conf. Ser.*, **7014**, 70143L
- Eiroa, C., Marshall, J. P., Mora, A., et al. 2013, *A&A*, **555**, A11
- Fulton, B. J., Rosenthal, L. J., Hirsch, L. A., et al. 2021, *ApJS*, **255**, 14
- Fusco, T., Rousset, G., Sauvage, J. F., et al. 2006, *Opt. Exp.*, **14**, 7515
- Gagné, J., Mamajek, E. E., Malo, L., et al. 2018, *ApJ*, **856**, 23
- Gaia Collaboration (Prusti, T., et al.) 2016, *A&A*, **595**, A1
- Gaia Collaboration (Brown, A. G. A., et al.) 2021, *A&A*, **649**, A1
- Galicher, R., Boccaletti, A., Mesa, D., et al. 2018, *A&A*, **615**, A92
- Grandjean, A., Lagrange, A. M., Keppler, M., et al. 2020, *A&A*, **633**, A44
- Groff, T. D., Kasdin, N. J., Limbach, M. A., et al. 2015, *SPIE Conf. Ser.*, **9605**, 96051C
- Haffert, S. Y., Bohn, A. J., de Boer, J., et al. 2019, *Nat. Astron.*, **3**, 749
- Keppler, M., Benisty, M., Müller, A., et al. 2018, *A&A*, **617**, A44
- Kervella, P., Arenou, F., Mignard, F., & Thévenin, F. 2019, *A&A*, **623**, A72
- Kervella, P., Arenou, F., & Thévenin, F. 2022, *A&A*, **657**, A7
- Langlois, M., Vigan, A., Moutou, C., et al. 2013, in *Proceedings of the Third AO4ELT Conference*, eds. S. Esposito, & L. Fini, 63
- Langlois, M., Gratton, R., Lagrange, A. M., et al. 2021, *A&A*, **651**, A71
- Lazzoni, C., Desidera, S., Marzari, F., et al. 2018, *A&A*, **611**, A43
- Lindgren, L., Klioner, S. A., Hernández, J., et al. 2021, *A&A*, **649**, A2
- Macintosh, B., Graham, J. R., Ingraham, P., et al. 2014, *Proc. Natl. Acad. Sci.*, **111**, 12661
- Macintosh, B., Graham, J. R., Barman, T., et al. 2015, *Science*, **350**, 64
- Marois, C., Lafrenière, D., Doyon, R., Macintosh, B., & Nadeau, D. 2006, *ApJ*, **641**, 556
- Marois, C., Correia, C., Véran, J.-P., & Currie, T. 2014, *IAU Symp.*, **299**, 48
- Mawet, D., Milli, J., Wahhaj, Z., et al. 2014, *ApJ*, **792**, 97
- Mesa, D., Gratton, R., Zurlo, A., et al. 2015, *A&A*, **576**, A121
- Mesa, D., Marino, S., Bonavita, M., et al. 2021, *MNRAS*, **503**, 1276
- Messina, S., Lanza, A. C., Malo, L., et al. 2017, *A&A*, **607**, A3
- Meyer, M. R., Amara, A., Reggiani, M., & Quanz, S. P. 2018, *A&A*, **612**, L3
- Nielsen, E. L., De Rosa, R. J., Macintosh, B., et al. 2019, *AJ*, **158**, 13
- Pavlov, A., Feldt, M., & Henning, T. 2008, *ASP Conf. Ser.*, **394**, 581
- Pawellek, N., Wyatt, M., Matrà, L., Kennedy, G., & Yelverton, B. 2021, *MNRAS*, **502**, 5390
- Perrot, C., Baudoz, P., Boccaletti, A., et al. 2018, *ArXiv e-prints* [arXiv:1804.01371]
- Racine, R., Walker, G. A. H., Nadeau, D., Doyon, R., & Marois, C. 1999, *PASP*, **111**, 587
- Soummer, R., Pueyo, L., & Larkin, J. 2012, *ApJ*, **755**, L28
- Steiger, S., Currie, T., Brandt, T. D., et al. 2021, *AJ*, **162**, 44
- Torres, C. A. O., Quast, G. R., da Silva, L., et al. 2006, *A&A*, **460**, 695
- Trifonov, T., Tal-Or, L., Zechmeister, M., et al. 2020, *A&A*, **636**, A74
- Vigan, A., Moutou, C., Langlois, M., et al. 2010, *MNRAS*, **407**, 71
- Vigan, A., Bonavita, M., Biller, B., et al. 2017, *A&A*, **603**, A3
- Vigan, A., Fontanive, C., Meyer, M., et al. 2021, *A&A*, **651**, A72
- Wright, E. L., Eisenhardt, P. R. M., Mainzer, A. K., et al. 2010, *AJ*, **140**, 1868
- Zúñiga-Fernández, S., Bayo, A., Elliott, P., et al. 2021, *A&A*, **645**, A30
- Zuckerman, B., Rhee, J. H., Song, I., & Bessell, M. S. 2011, *ApJ*, **732**, 61
- Zurlo, A., Vigan, A., Mesa, D., et al. 2014, *A&A*, **572**, A85